Letter

Interplay of charge and spin fluctuations in a Hund's coupled impurity

Victor Drouin-Touchette [1], Elio J. König [2,*] Yashar Komijani [3] and Piers Coleman [1,4]
[1] Center for Materials Theory, Department of Physics and Astronomy, Rutgers University, Piscataway, New Jersey 08854, USA
[2] Max-Planck Institute for Solid State Research, 70569 Stuttgart, Germany
[3] Department of Physics, University of Cincinnati, Cincinnati, Ohio 45221-0011, USA
[4] Department of Physics, Royal Holloway, University of London, Egham, Surrey TW20 0EX, United Kingdom

(Received 22 April 2022; revised 8 September 2022; accepted 9 September 2022; published 20 October 2022)

In Hund's metals, the local ferromagnetic interaction between orbitals leads to an emergence of complex electronic states with large and slowly fluctuating magnetic moments. Introducing the Hund's coupled mixed-valence quantum impurity, we gain analytic insight into recent numerical renormalization group studies. We show that valence fluctuations drastically impede the development of a large fluctuating moment over a wide range of temperatures and energy, characterized by quenched orbital degrees of freedom and a singular logarithmic behavior of the spin susceptibility $\chi''_{\rm sp}(\omega) \propto [\omega \ln(\omega/T_K^{\rm eff})^2]^{-1}$, closely resembling power-law scaling $\chi''_{\rm sp}(\omega) \sim \omega^{-\gamma}$. Finally, we outline how such singular spin fluctuations can play an important role in generating a superconducting state through Hund's driven Cooper pairing.

DOI: 10.1103/PhysRevResearch.4.L042011

Introduction.—The concept of Hund's metals was first introduced in the context of iron-based superconductors [1–3], with the nomenclature now being extended to include the ruthenates [4–6]. In both cases, the local physics is characterized by electronic shells that are one filling away from half-filling [7,8]. Although the onsite Coulomb interaction U is the largest scale, its effect is overshadowed by that of the ferromagnetic interorbital Hund interaction [9]. This class of materials presents an intermediate paramagnetic regime dominated by slowly fluctuating high-spin configurations [10–12] and largely suppressed Fermi liquid coherence scales, leading to anomalous transport properties [13–15]. It has been speculated that Cooper pairing emerges out of this intermediate state in iron-based compounds [16–22].

The link between large moments generated by Hund's coupling and the exponential reduction of Fermi liquid scales in Kondo impurity models has been studied extensively [23–28]. However, the physical valence of Fe or Ru atoms in Hund's metals deviates from half-filled shells. This has led to a vigorous interest in doped multiorbital models, where an intermediate coupling non-Fermi-liquid fixed point was pointed out through analytical [29] and NRG studies [30–32] for the $S = 1$, three orbitals system. Most of these studies were performed for exactly two electrons among three orbitals; few explicitly addressed charge fluctuations out of this state [9,33].

*elio.j.koenig@gmail.com

Motivated by the potentially new physics in the mixed valence regime, here we extend our previous work on the Hund-Kondo impurity [28]. This, coupled with the unique property of the large-N self-consistent equations which enable a direct access to real frequency correlation functions [34], has led us to study in detail the dynamical properties of the intermediate regime generated by Hund's coupling.

In this Letter, we show that the treatment of charge and spin dynamics on equal footing within the dynamical large-N approach [28,34–42] leads to new insight into the dynamical properties of hole doped multi-orbital impurities. Based on computed thermodynamic quantities, we unveil the complete phase diagram [see Fig. 1] as a function of impurity occupancy. Furthermore, we characterize the large emergent moment regime [28] as one with spin-orbital separation [43]. The spin susceptibility shows logarithmic corrections due to the extremely slow approach to Kondo screening, reminiscent of the low-energy properties of the underscreened Kondo model [44–47]. At a strongly renormalized Kondo temperature $T_K^{\rm eff} \ll T_K^0$, the charge degrees of freedom eventually gap out, resulting in a local Fermi liquid. The scaling of the local spin susceptibility in the spin-orbital separated regime is found to exhibit quasi-power-law scaling due to the unusually strong logarithmic corrections.

Model.—We consider a degenerate three-orbital impurity model, in analogy to the t_{2g} orbital subset generated due to the tetrahedral environment around the iron atoms in Fe-based Hund's metals. Mixed-valence states are included via a Hund-Anderson model. We take the limit of $U \to \infty$, such that the Coulomb interaction enforces a "no double occupancy" rule for each of the m orbitals. This is a valid limit away from exactly half-filling where we can focus on the role of Hund's coupling. This is enforced through the use of Hubbard operators [48] for each orbital, which transform the K empty states $|d^0 : a, m\rangle$ into the N magnetic states $|d^1 : \alpha, m\rangle$ filled with

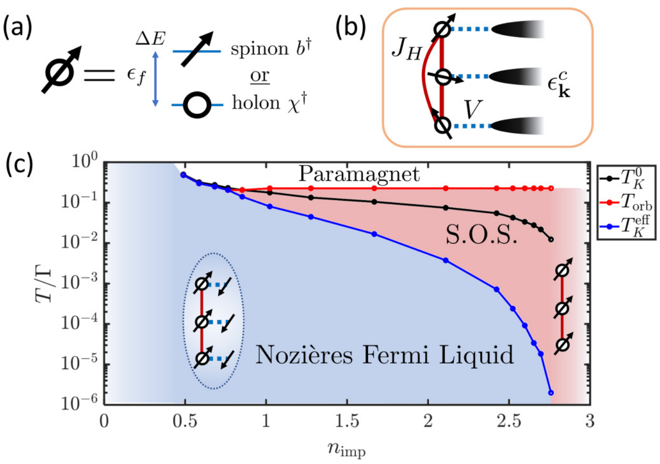

FIG. 1. (a)–(b) Schematic mixed valence states and of the Hund-coupled three-orbital Anderson model, referring to Eq. (2). (c) Phase diagram obtained as a function of total impurity filling $n_{\rm imp}$ (left side is holon dominated). $T_{\rm orb}$ and $T_K^{\rm eff}$ are crossover temperatures where the specific heat c_v has a local maxima, as in Fig. 2. Generically, screening occurs in two steps. The formation of a large emergent fluctuating moment, while orbital degrees of freedom are quenched, occurs at $T_{\rm orb}$. In this spin-orbital separated (SOS) regime, we see a Curie-like spin susceptibility $\chi_{\rm sp} \sim \mu^2/T$ while the orbital susceptibility reaches a plateau. Then, at $T_K^{\rm eff} \ll T_K^0$, with T_K^0 the bare Kondo temperature for $J_H = 0$, the large moment is screened and forms a local Fermi liquid. $\Gamma = \pi\rho V^2$ is the bare hybridization width.

local d electrons for each orbital m. In the large-N formalism, local moments transform as spin-S representations of SU(N), and there are $K = 2S$ electronic channels present to maintain perfect screening. Schwinger bosons $X^{(m)}_{\alpha,\beta} = b^\dagger_{m\alpha} b_{m\beta}$ are used to express the spin degrees of freedom through spinons $b^\dagger$ which form a symmetric representation of the spins. Together with the use of slave fermions (holons $\chi^\dagger$), Hubbard operators can faithfully be represented as

$$\begin{aligned} X^{(m)}_{\alpha,a} &\equiv |d^1 : \alpha, m\rangle\langle d^0 : a, m| = b^\dagger_{m\alpha}\chi_{ma}, \\ X^{(m)}_{a,\alpha} &\equiv |d^0 : a, m\rangle\langle d^1 : \alpha, m| = \chi^\dagger_{ma} b_{m\alpha}, \\ X^{(m)}_{a,b} &\equiv |d^0 : a, m\rangle\langle d^0 : b, m| = \chi^\dagger_{ma}\chi_{mb}, \\ X^{(m)}_{\alpha,\beta} &\equiv |d^1 : \alpha, m\rangle\langle d^1 : \beta, m| = b^\dagger_{m\alpha} b_{m\beta}, \end{aligned} \tag{1}$$

while the Hamiltonian is itself expressed as $H = \sum_m H_c^{(m)} + \sum_m H_{\rm K}^{(m)} + H_{\rm H}$, with individual terms

$$H_c^{(m)} = \sum_{\mathbf{k}} \epsilon^c_{\mathbf{k}} c^\dagger_{\mathbf{k}m\alpha a} c_{\mathbf{k}m\alpha a}, \tag{2a}$$

$$H_{\rm K}^{(m)} = V\left(c^\dagger_{0m\alpha a} X^{(m)}_{a,\alpha} + X^{(m)}_{\alpha,a} c_{0m\alpha a}\right) + \epsilon_f X^{(m)}_{a,a}, \tag{2b}$$

$$H_{\rm H} = -\frac{J_H}{N}\sum_m X^{(m)}_{\alpha\beta} X^{(m+1)}_{\beta\alpha}. \tag{2c}$$

A visual representation of the mixed valence states and the Hund-Anderson model is presented at Fig. 1(a). Here, V is the hybridization between conduction electrons and the Hubbard operators corresponding to adding or removing an impurity electron ($\Gamma = \pi\rho V^2$ is the bare hybridization width). We denote the energy of a hole as ϵ_f which, when tuned, leads to different $n_{\rm imp}$ as the average valence of each state is changed. A more realistic model which includes crystal field splitting effect between the orbitals could be implemented by tuning $\epsilon_f^{(m)}$ for each orbital independently [49,50]. This would lead to orbital differentiation [51,52], and is beyond the scope of our work [53]. The Hund's term $H_{\rm H}$ can be treated through a Hubbard-Stratonovich decoupling in the hopping channel:

$$H_{\rm H} \to \sum_m [\bar{\Delta}_m (b^\dagger_{m+1,\alpha} b_{m\alpha}) + h.c.] + \frac{N|\Delta_m|^2}{J_H}. \tag{3}$$

A mean-field equation relates J_H to the spinon gap Δ, such that generically $\Delta/J_H = \langle \sum_m b^\dagger_{m+1} b_m \rangle$ [28]. If J_H is large enough to generate a finite Δ, their relationship will be such that $N\Delta = 2Sn_{\rm imp}J_H$ for $T \gg T_K^0$. Furthermore, the total charge

$$Q_m = \sum_\alpha b^\dagger_{m\alpha} b_{m\alpha} + \sum_a \chi^\dagger_{ma}\chi_{ma} = 2S, \tag{4}$$

at each orbital commutes with the Hubbard operators and is a conserved quantity, setting the size of the local moments. This is a constraint on the spinons/holons, enforced through a common Lagrange multiplier λ. In the large-N limit, the dynamics of holons and spinons is dominated by the noncrossing Feynman diagrams, which leads to the self-energy equations

$$\Sigma_\chi(\tau) = g_{c,0}(-\tau)G_B(\tau), \;\; \Sigma_B(\tau) = -kg_{c,0}(\tau)G_\chi(\tau), \tag{5}$$

where $k = K/N = 2S/N$ and $g_{c,0}(z) = \sum_{\mathbf{k}} [z - \epsilon^c_{\mathbf{k}}]^{-1}$ corresponds to the conduction electron's bare propagator for imaginary frequencies z. Equations (5) are solved self-consistently together with the Dyson equations $G_b(z) = \sum_m G_B(m, z) = \sum_p [z - \epsilon_p - V^2\Sigma_b(z)]^{-1}$ and $G_\chi(z) = [z - \epsilon_f^* - V^2\Sigma_\chi(z)]^{-1}$. Here, we used the following definitions: $G_B(m, z)$ is the spinon's Green's function on orbital m, $\epsilon_p = (\lambda - 2\Delta\cos p)$ is the energy of the spinon states, and $\epsilon_f^* = \lambda + \epsilon_f$ is the effective holon energy. We also defined the chirality $p = 0, \pm 2\pi/3$ which denotes the chosen Hund energy levels such that $p = 0$ is the aligned state (maximum total spin). λ and Δ are adjusted to fit the constraint of Eq. (4) and the mean-field relation between J_H and Δ.

Thermodynamic and dynamical observables are obtained from the Green's functions [28,34,35]. Notably, the impurity entropy $S_{\rm imp}(T)$ can be extracted exactly in the large-N limit [54,55] and is given by

$$\begin{aligned} S_{\rm imp} = -{\rm Tr}\int \frac{d\omega}{\pi}\bigg(&\frac{\partial n_B}{\partial T}\left[{\rm Im}\,\ln\left(-G_B^{-1}\right) + G_B'\Sigma_B''\right] \\ &+ \gamma\frac{\partial n_F}{\partial T}\left[{\rm Im}\,\ln\left(-G_\chi^{-1}\right) + G_\chi'\Sigma_\chi'' - g_{c,0}''\tilde{\Sigma}_c'\right]\bigg), \end{aligned} \tag{6}$$

where the trace is over all α and a spin and channel indices and chiralities p, and $\tilde{\Sigma}_c(\tau) = G_\chi(-\tau)G_B(\tau)$. G_ξ' is the real part of the retarded Green's function while Σ_ξ'' is the imaginary part of the self-energy for the corresponding fields. From this closed form, we can extract the specific heat as $c_{v,{\rm imp}} = T\partial S_{\rm imp}/\partial T$.

Summary of results.—In the absence of Hund's coupling, one simply recovers three copies of infinite-U Anderson models. In this case, the presence of holons (decreasing $n_{\rm imp}$) increases the bare Kondo temperature $T_K^0 \sim De^{-1/J_K^0\rho} \sim$

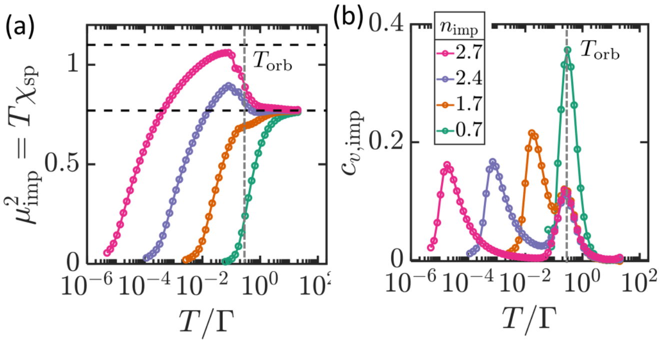

FIG. 2. (a) The impurity's local moment $\mu^2_{\rm imp}$ obtained from the spin susceptibility, for varied impurity occupations $n_{\rm imp}$. The large emergent moment, seen as a low-temperature higher plateau, is destroyed as more holons are added, following the trend of Fig. 1. (b) The specific heat $c_{v,\rm imp}$, obtained from the closed form of the entropy for the multiorbital Anderson model, see Eq. (6). Both $T_{\rm orb}$ and $T_K^{\rm eff}$ are crossovers associated with c_v peaks. Dashed lines are high and intermediate temperature limits for the $\mu^2_{\rm imp}$, obtained in Ref. [28].

$D\exp(-|\epsilon_f|/\Gamma)$ for a fixed hybridization width Γ, conduction electron bandwidth D, and effective holon energy ϵ_f^*. The holon occupation number n_χ can be absorbed through a Gutzwiller renormalization of the hybridization $V \to \tilde{V} \sim V\sqrt{\langle n_\chi\rangle}$ [48], such that as $n_\chi \to 0$, $T_K^0 \to 0$ exponentially. Solving the self-energy equations for $J_H = 0$ leads to this expected trend, shown in black in Fig. 1(c) [56].

For a finite Hund's coupling, the situation changes drastically. The emergence of an intermediate large moment phase in the Kondo limit is consistent with our previous work on the Hund-Kondo model [28]. We can now connect this phase continuously throughout the hole-doped regime. At some critical holon doping, there is no longer enough local moments to lock together; the two-step Kondo screening reverts to a single step Kondo crossover. The obtained phase diagram of Fig. 1 is consistent with other NRG + DMFT studies [9] of hole-doped multiorbital impurity models.

In Fig. 2, we present the thermodynamic measurements of the total impurity's magnetic moment $\mu^2 \sim T\chi_{\rm sp}$ as well as the impurity specific heat for select impurity occupations $n_{\rm imp}$ throughout the entire temperature range. For Kondo-like systems ($n_{\rm imp} = 2.7$) there is a clear nonmonoticity in the local moment, signaling the intermediate formation of an emergent large moment due to Hund's coupling. As the holon occupancy increases, there are less spinons in the system and the emergent moment can no longer form; the shoulder disappears at $n_{\rm imp} \approx 0.7$. In the specific heat, this disappearance of the intermediate phase is seen as the low and high temperature crossover features merge to become one as $n_{\rm imp} = 0.7$, where single-step Kondo screening occurs.

Previous works [9,31,32,43,57] have characterized the intermediate large moment phase as a regime with spin-orbital separation. We can take advantage of the Hubbard operators' description in terms of spinons and holons to write composite orbital operators. This procedure would not be possible with virtual holons, as obtained in past treatments of the Hund-Kondo model [28]. The finite holon occupancy in the Hund-Anderson model leads to a well-defined orbital degrees of freedom. Starting with the total impurity spin operators at imaginary time τ, described as $S_{\alpha\beta}(\tau) = \sum_m X^{(m)}_{\alpha\beta}(\tau) = \sum_m b^\dagger_{m\alpha}(\tau)b_{m\beta}(\tau)$ (α, β are SU(N) spin states), we then harness the SO(3) orbital symmetry and describe impurity orbital operators $\hat{L}_\gamma$ ($\gamma = x, y, z$ corresponding to the three degenerate orbitals) as $\hat{L}_\gamma = (1/NK)\sum_{mm'\alpha\alpha} X^{(m)}_{\alpha\alpha}(L_\gamma)_{mm'}X^{(m')}_{\alpha\alpha}$. The L_γ are generators of the SO(3) group [58] such that $(L_\gamma)_{mm'} = i\epsilon_{\gamma mm'}$ with ϵ_{ijk} the antisymmetric Levi-Civita tensor. The spin and orbital susceptibilities in the large-N limit can thus be expressed as

$$\chi_{\rm sp}(\tau) = \frac{1}{N^2}\sum_\gamma\sum_{\alpha\beta}\left\langle S^{(\gamma)}_{\alpha\beta}(\tau)S^{(0)}_{\beta\alpha}(0)\right\rangle_c \to \sum_m G_B(m,\tau)G_B(-m,-\tau), \tag{7a}$$

$$\chi_{\rm orb}(\tau) = \frac{1}{3}\sum_\gamma\langle\hat{L}_\gamma(\tau)\hat{L}_\gamma(0)\rangle_c \to \frac{1}{K}\left(\frac{\Delta}{J_H}\right)^2 G_\chi(\tau)G_\chi(-\tau), \tag{7b}$$

where $\langle\cdots\rangle_c$ denotes averages over connected diagrams. The derivation of the expression for the spin susceptibility is identical to our previous work [28]. The expression for the orbital susceptibility is obtained through two essential steps. Firstly, after the $\hat{L}_\gamma$ operators are represented in terms of Hubbard operators, Wick contractions over the bosonic and fermionic degrees of freedom leaves only two relevant contributions in the large-N limit. Secondly, the absence of holon interorbital hopping leads to many terms being zero. Summing over $\gamma = x, y, z$ leads to the quoted result. The full expression for the dynamical susceptibilities in real frequency are presented in the Supplemental Materials [56], as well as further details on this derivation. Note that the orbital susceptibility has a $1/K$ factor reduction compared to $\chi_{\rm sp}$; we nevertheless can plot $K\chi_{\rm orb}$ and obtain valuable insight. The static components of these susceptibilities, $\chi_{\rm orb}(\tau = 0)$ and $\chi_{\rm sp}(\tau = 0)$, are shown in panel (a) of Fig. 3. The clear splitting of both susceptibilities at $T_{\rm orb}$, and the subsequent plateau in $\chi_{\rm orb}$, signals the formation of the large moment and the separation of spin and orbital scales (SOS). Throughout this regime, orbital and charge fluctuations are nearly frozen while the spin susceptibility remains Curie-like.

Dynamical susceptibilities.—The emergent moment regime has clear thermodynamic attributes, as described above (see Fig. 2). Further insight into this phase is provided by the dynamical spin and orbital susceptibilities, as defined in Eqs. (7). We show these in Fig. 3 for two different total impurity valences. It can be clearly seen that at high frequencies, both spin and orbital degrees of freedom fluctuate freely. For $\omega < T_{\rm orb}$, the lower-energy high-spin configurations split off, which is associated with the separation of the spin and orbital dynamical susceptibility. In this regime, the charge fluctuations freeze and the valence stabilizes below $T_{\rm orb}$; this quenching of orbital degrees of freedom leads to the decrease in $\chi''_{\rm orb}$ with respect to $\chi''_{\rm sp}$.

From Fig. 3, we see that, for many decades in frequency between $T_K^{\rm eff}$ and $T_{\rm orb}$, the spin susceptibility seems to grow in a power-law $\chi_{\rm sp} \sim \omega^{-\gamma}$ (dot-dashed green line). In

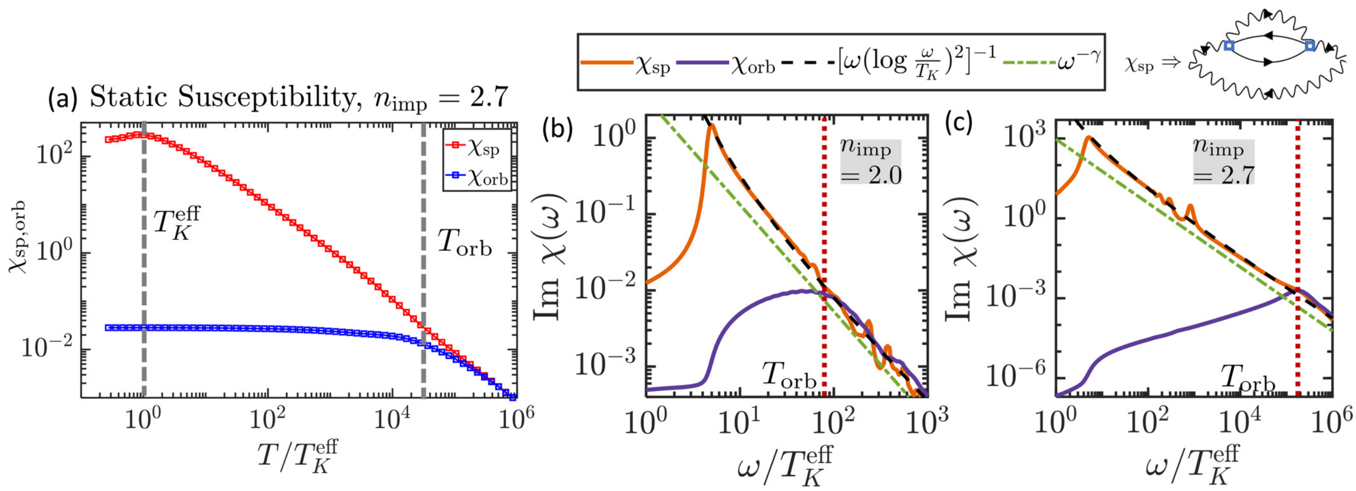

FIG. 3. (a) Static spin and orbital susceptibilities for $n_{\rm imp} = 2.7$, showing a clear separation at $T_{\rm orb}$ below which the Curie-like $\chi_{\rm sp} \sim \mu^2/T$ spin susceptibility is in stark constrast to the constant $\chi_{\rm orb}$. (b)–(c) Imaginary part of the dynamical spin and orbital susceptibilities, Eqs. (7), presented for different occupations of the three-orbital impurity: $n_{\rm imp} = 2$ and $n_{\rm imp} = 2.7$ from left to right. The value of the Hund coupling $J_H/D = 0.37$ is fixed, and results are presented for $T \simeq 0.1T_K^{\rm eff}$. The dashed black line corresponds to the derived second-order perturbation scaling of the spinon susceptibility, Eqs. (8), while the dot-dashed green line is the quasi-power-law form of Eq. (10) (with small offset for readability). At the top right, we show the second order contribution to $\chi_{\rm sp}$ which leads to the logarithmic scaling. Conduction electron (spinon) Green's functions are represented as solid (wavy) lines.

Kondo impurity problems, such behavior is often indicative of non-Fermi-liquid fixed points [31,32], for example in the 2-channel spin-1/2 Kondo model [59–64]. Closer examination reveals that this is not the case in this system, having maintained perfect screening ($2S = K$) throughout. Instead, we find a good agreement at intermediate temperatures and frequencies with the scaling

$$\chi''_{\rm sp}(\omega) = \frac{\left(J_K^{\rm eff}\rho\right)^2}{\omega} \propto \left(\omega\left[\ln\left(\frac{\omega}{T_K^{\rm eff}}\right)\right]^2\right)^{-1}. \quad (8)$$

Here we cover the basic steps of this derivation and leave the details for the supplementary materials [56]. Firstly, we solve a single iteration [28] of the self-energy equations of Eq. (5) analytically, starting from the bare Green's functions $G_{\xi,0}(z)$. This leads to an expression for the renormalized Kondo temperature $T_K^{\rm eff}$. Furthermore, for $T_K^{\rm eff} \leqslant \max(\omega, T) \leqslant T_{\rm orb}$, we can map the mixed valence problem onto a Kondo problem, leading to an effective holon propagator $\tilde{G}_\chi(\omega) = -J_K^{\rm eff}(\omega)$, with

$$\frac{1}{\rho J_K^{\rm eff}(\omega)} \simeq \ln\left(\frac{\max(\omega, T)}{T_K^{\rm eff}}\right). \quad (9)$$

Secondly, after having obtained this effective running Kondo coupling, we proceed in a second-order perturbation in $J_K^{\rm eff}$ of the spinon bubble of the spin susceptibility [65]. This is shown in the top right of Fig. 3. Blue boxes corresponds to factors of $\rho J_K^{\rm eff}$, and the calculation of this diagram leads to the scaling presented in Eq. (8). One can see in Fig 3 that it agrees perfectly within the intermediate regime $T_K^{\rm eff} < \omega < T_{\rm orb}$ with only $T_K^{\rm eff}$ as an input parameter. A downturn is observed at lower frequencies consistent with Im $\chi_{\rm sp} \propto \omega$ in the Fermi liquid regime. This scaling holds for all $n_{\rm imp}$ of the phase diagram where the SOS phase is present.

In the SOS regime, the large separation of scales between $T_K^{\rm eff}$ and $T_{\rm orb}$ leads to a peculiar observation about Eq. (8). For intermediate frequencies, we find that a quasi-power-law form for the spin susceptibility,

$$\chi_{\rm pwl} \sim \omega^{-\gamma} \quad \text{and} \quad \gamma = 1 - 2/\ln\left(\frac{T_K^{\rm eff}}{\mathcal{D}}\right), \quad (10)$$

with $\mathcal{D} = \min(\Gamma, T_{\rm orb})$, is indistinguishable from the form with the logarithmic correction. These two start to deviate as one gets to very small frequencies $\omega \ll \mathcal{D}$ [56], which results in the upturn seen close to $T_K^{\rm eff}$ in Fig. 3. For very small $T_K^{\rm eff}/T_{\rm orb}$, due to strong Hund's coupling and the resulting nearly frozen charge fluctuations, the slow logarithmic scaling presents itself as this quasi-power-law for many decades in frequency. We find that, for a given fixed $J_H/D = 0.37$, $\gamma \simeq 1.2$ for $n_{\rm imp} = 2.7$ and $\gamma \simeq 1.4$ for $n_{\rm imp} = 2.0$. This exponent γ changes continuously as $n_{\rm imp}$ is varied.

We note that $\chi''_{\rm sp} \sim \omega^{-1.2}$ was seen in a different but related model [31,32], and was invoked in phenomenological modeling of the spin-fluctuation-induced Cooper pairing in the iron-based superconductors [66,67]. In those references, the presence of a putative soft boson with $\chi''_{\rm sp} \sim \omega^{-1.2}$, when included in a Eliashberg approach, led to a superconducting instability with universal properties relevant for the iron-based superconductors, but the origin of this mode was an open question. Our results provide a tentative identification of this mode in terms of Hund's driven Kondo screening.

Eliashberg approach.—We can extend these arguments to the singular local spin susceptibility obtained here. Firstly, we can extract two contributions to the interaction kernel for the

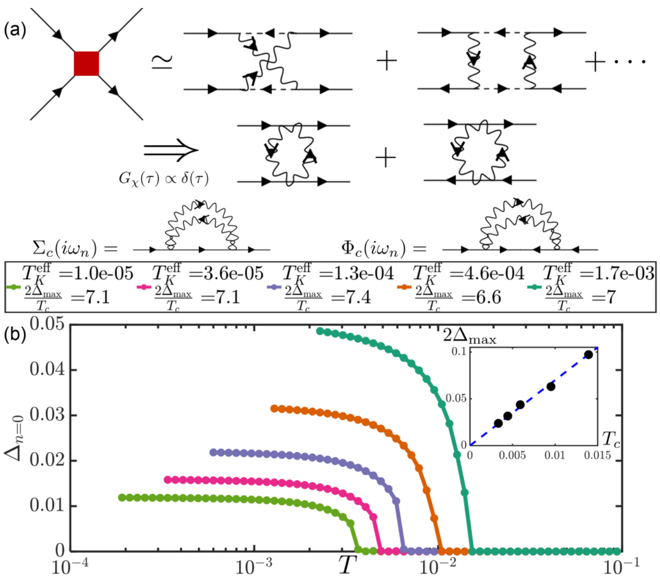

FIG. 4. (a) In red, interaction kernel for the conduction electrons. In the Schwinger-boson representation, there are two contributions. For temperatures below $T_{\rm orb}$, the holons are nearly instantaneous propagators and the two diagrams can be simplified. A spinon bubble is then the contribution to the pairing vertex Φ_c and fermionic self-energy Σ_c. Holon propagators are represented by dashed lines, while conduction electrons (spinons) are represented by full (wavy) lines. (b) Solving Eq. (11) with $\lambda = \chi''_{\rm sp}$, with different $T_K^{\rm eff}$ chosen. The inset shows $2\Delta_{\rm max}$ vs T_c for the presented curves, along with $2\Delta_{\rm max} \propto 7.0T_c$ in dashed blue.

conduction electrons at the $O(1/N^2)$ level, shown in Fig. 4: a normal and an anomalous contribution, respectively. In the SOS regime, the quenching of the local moments, which also leads to the apparent quasi-power-law behavior, means that the holon's propagators can be approximated as instantaneous $G_\chi \propto \delta(\tau)$ [68]. Simplifying the two contributions leads to a pairing vertex and fermionic self-energy of equal magnitude, both occurring through $\chi''_{\rm sp}$; this acts as our soft boson.

Following the work of Ref. [66], we can express the Eliashberg equations [69–73] for the pairing vertex $\Phi_c(\omega_n)$ and the fermionic self-energy $\Sigma_c(\omega_n)$ in a closed form. These can be factorized using the pairing gap function $\Delta(\omega_n) = \Phi(\omega_n)\omega_n/(\omega_n + \Sigma(\omega_n))$, leading to a closed equation for $\Delta(\omega_n) \equiv \Delta_n$:

$$\Delta_n = \pi T \sum_{\omega_m} \frac{\lambda(\omega_m - \omega_n)}{\sqrt{\omega_m^2 + \Delta_m^2}} \left(\Delta_m - \Delta_n \frac{\omega_m}{\omega_n} \right), \tag{11}$$

where $\omega_n = \pi T(2n+1)$ is the nth fermionic Matsubara frequency and $\lambda(\Omega) \sim \chi''_{\rm sp}(\Omega)$ carries the effect of the spin fluctuation bubble. Note that this form only holds for the intermediate frequency and temperature window of $T_K^{\rm eff} < T, \Omega < T_{\rm orb}$. This can then be used to obtain $\Sigma(\omega_n)$. Solving Eq. (11) shows that as the temperature is lowered, a finite $\Delta_n \neq 0$ develops below T_c. In Fig. 4(b), we show the maximum gap, achieved at $n = 0$, as a function of temperature. The critical temperature and the maximal gap $\Delta_{\rm max} = \Delta_0(T \to 0)$ are seen to scale with $T_K^{\rm eff}$ and T_c. For all $T_K^{\rm eff}$ studied, the SOS window is large enough to generate a superconducting state within the Eliashberg approach. Furthermore, we find that $2\Delta_{\rm max}/T_c \sim 7.0 \pm 0.5$ for a wide range of $T_K^{\rm eff}/T_{\rm orb}$, close to the universal value observed in Ref. [74].

Conclusion.—We have shown that the dynamical large-N approach can capture the destruction of the Hund's coupled emergent large moment due to hole doping. Furthermore, we show that the intermediate regime is well described through the concept of spin-orbital separation (SOS) [9,43]. In this phase, the dynamical spin susceptibility has a logarithmic component due to the nearly frozen charge fluctuations, which presents itself as a quasi-power-law for an extended frequency range because $T_K^{\rm eff} \ll T_{\rm orb}$. The non-Fermi-liquid-like features in the emergent moment regime can be continuously connected to the integer valence limit. We have also shown how the singular aspects of this spin susceptibility can be included in a Eliashberg treatment and lead to a superconducting state with quasiuniversal properties reminiscent of the iron-based superconductors.

Acknowledgments.—VDT would like to thank Elias Walter, Seung-Sup B. Lee, Andreas Weichselbaum, Jan von Delft, Fabian Kugler, Abhishek Kumar, and Tsung-Han Lee for illuminating discussions. We also acknowledge useful discussions with Thomas Schäfer. This work was supported by the U.S. Department of Energy, Office of Basic Energy Sciences, under Contract No. DE-FG02-99ER45790 (VDT, PC) and the Fonds de Recherche Québécois en Nature et Technologie (VDT).

[1] K. Haule and G. Kotliar, Coherence–incoherence crossover in the normal state of iron oxypnictides and importance of Hund's rule coupling, New J. Phys. **11**, 025021 (2009).
[2] Z. Yin, K. Haule, and G. Kotliar, Fractional power-law behavior and its origin in iron-chalcogenide and ruthenate superconductors: Insights from first-principles calculations, Phys. Rev. B **86**, 195141 (2012).
[3] L. Fanfarillo and E. Bascones, Electronic correlations in Hund metals, Phys. Rev. B **92**, 075136 (2015).
[4] H. T. Dang, J. Mravlje, A. Georges, and A. J. Millis, Electronic correlations, magnetism, and Hund's rule coupling in the ruthenium perovskites $SrRuO_3$ and $CaRuO_3$, Phys. Rev. B **91**, 195149 (2015).
[5] X. Deng, K. Haule, and G. Kotliar, Transport Properties of Metallic Ruthenates: A DFT+DMFT Investigation, Phys. Rev. Lett. **116**, 256401 (2016).
[6] Y. Wang, C.-J. Kang, H. Miao, and G. Kotliar, Hund's metal physics: From $SrNiO_2$ to $LaNiO_2$, Phys. Rev. B **102**, 161118(R) (2020).
[7] L. de' Medici, Hund's coupling and its key role in tuning multiorbital correlations, Phys. Rev. B **83**, 205112 (2011).
[8] A. Georges, L. de Medici, and J. Mravlje, Strong correlations from Hund's coupling, Annu. Rev. Condens. Matter Phys. **4**, 137 (2013).
[9] K. M. Stadler, G. Kotliar, A. Weichselbaum, and J. von Delft, Hundness versus mottness in a three-band Hubbard–Hund

model: On the origin of strong correlations in Hund metals, Ann. Phys. **405**, 365 (2019).

[10] P. Werner, E. Gull, M. Troyer, and A. J. Millis, Spin Freezing Transition and Non-Fermi-Liquid Self-Energy in a Three-Orbital Model, Phys. Rev. Lett. **101**, 166405 (2008).

[11] C. Watzenböck, M. Edelmann, D. Springer, G. Sangiovanni, and A. Toschi, Characteristic Timescales of the Local Moment Dynamics in Hund's Metals, Phys. Rev. Lett. **125**, 086402 (2020).

[12] P. Hansmann, R. Arita, A. Toschi, S. Sakai, G. Sangiovanni, and K. Held, Dichotomy between Large Local and Small Ordered Magnetic Moments in Iron-Based Superconductors, Phys. Rev. Lett. **104**, 197002 (2010).

[13] F. Hardy, A. Böhmer, D. Aoki, P. Burger, T. Wolf, P. Schweiss, R. Heid, P. Adelmann, Y. Yao, G. Kotliar, J. Schmalian, C. Meingast, Evidence of Strong Correlations and Coherence-Incoherence Crossover in the Iron Pnictide Superconductor KFe_2As_2, Phys. Rev. Lett. **111**, 027002 (2013).

[14] F. Hardy, A. Böhmer, L. de'Medici, M. Capone, G. Giovannetti, R. Eder, L. Wang, M. He, T. Wolf, P. Schweiss, R. Heid, A. Herbig, P. Adelmann, R. A. Fisher, C. Meingast, Strong correlations, strong coupling, and s-wave superconductivity in hole-doped $BaFe_2As_2$ single crystals, Phys. Rev. B **94**, 205113 (2016).

[15] R. Yang, Z. Yin, Y. Wang, Y. Dai, H. Miao, B. Xu, X. Qiu, and C. C. Homes, Observation of an emergent coherent state in the iron-based superconductor KFe_2As_2, Phys. Rev. B **96**, 201108(R) (2017).

[16] G. R. Stewart, Superconductivity in iron compounds, Rev. Mod. Phys. **83**, 1589 (2011).

[17] H. Hosono, A. Yamamoto, H. Hiramatsu, and Y. Ma, Recent advances in iron-based superconductors toward applications, Mater. Today **21**, 278 (2018).

[18] C. M. Puetter and H.-Y. Kee, Identifying spin-triplet pairing in spin-orbit coupled multi-band superconductors, EPL (Europhysics Letters) **98**, 27010 (2012).

[19] S. Hoshino and P. Werner, Superconductivity from Emerging Magnetic Moments, Phys. Rev. Lett. **115**, 247001 (2015).

[20] O. Vafek and A. V. Chubukov, Hund Interaction, Spin-Orbit Coupling, and the Mechanism of Superconductivity in Strongly Hole-Doped Iron Pnictides, Phys. Rev. Lett. **118**, 087003 (2017).

[21] A. K. C. Cheung and D. F. Agterberg, Superconductivity in the presence of spin-orbit interactions stabilized by hund coupling, Phys. Rev. B **99**, 024516 (2019).

[22] P. Coleman, Y. Komijani, and E. J. König, Triplet Resonating Valence Bond State and Superconductivity in Hund's Metals, Phys. Rev. Lett. **125**, 077001 (2020).

[23] J. Schrieffer, The Kondo effect–the link between magnetic and nonmagnetic impurities in metals?, J. Appl. Phys. **38**, 1143 (1967).

[24] I. Okada and K. Yosida, Singlet ground state of the localized d-electrons coupled with conduction electrons in metals, Prog. Theor. Phys. **49**, 1483 (1973).

[25] P. Nozières and A. Blandin, Kondo effect in real metals, J. de Physique **41**, 193 (1980).

[26] C. Jayaprakash, H. R. Krishna-Murthy, and J. W. Wilkins, Two-Impurity Kondo Problem, Phys. Rev. Lett. **47**, 737 (1981).

[27] A. H. Nevidomskyy and P. Coleman, Kondo Resonance Narrowing in d-and f-Electron Systems, Phys. Rev. Lett. **103**, 147205 (2009).

[28] V. Drouin-Touchette, E. J. König, Y. Komijani, and P. Coleman, Emergent moments in a hund's impurity, Phys. Rev. B **103**, 205147 (2021).

[29] C. Aron and G. Kotliar, Analytic theory of Hund's metals: A renormalization group perspective, Phys. Rev. B **91**, 041110(R) (2015).

[30] A. Horvat, R. Zitko, and J. Mravlje, Non-Fermi-liquid fixed point in multi-orbital Kondo impurity model relevant for Hund's metals, arXiv:1907.07100.

[31] Y. Wang, E. Walter, S. S. B. Lee, K. M. Stadler, J. von Delft, A. Weichselbaum, and G. Kotliar, Global Phase Diagram of a Spin-Orbital Kondo Impurity Model and the Suppression of Fermi-Liquid Scale, Phys. Rev. Lett. **124**, 136406 (2020).

[32] E. Walter, K. M. Stadler, S. S. B. Lee, Y. Wang, G. Kotliar, A. Weichselbaum, and J. von Delft, Uncovering Non-Fermi-Liquid Behavior in Hund Metals: Conformal Field Theory Analysis of an SU (2)× SU (3) Spin-Orbital Kondo Model, Phys. Rev. X **10**, 031052 (2020).

[33] S. Ryee, S. Choi, and M. J. Han, Frozen spin ratio and the detection of Hund correlations, arXiv:2207.10421.

[34] Y. Komijani and P. Coleman, Model for a Ferromagnetic Quantum Critical Point in a 1D Kondo Lattice, Phys. Rev. Lett. **120**, 157206 (2018).

[35] J. Rech, P. Coleman, G. Zarand, and O. Parcollet, Schwinger Boson Approach to the Fully Screened Kondo Model, Phys. Rev. Lett. **96**, 016601 (2006).

[36] Y. Komijani and P. Coleman, Emergent Critical Charge Fluctuations at the Kondo Breakdown of Heavy Fermions, Phys. Rev. Lett. **122**, 217001 (2019).

[37] J. Wang, Y.-Y. Chang, C.-Y. Mou, S. Kirchner, and C.-H. Chung, Quantum phase transition in a two-dimensional Kondo-Heisenberg model: A dynamical Schwinger-boson large-N approach, Phys. Rev. B **102**, 115133 (2020).

[38] B. Shen, Y. Zhang, Y. Komijani, M. Nicklas, R. Borth, A. Wang, Y. Chen, Z. Nie, R. Li, X. Lu *et al.*, Strange-metal behaviour in a pure ferromagnetic Kondo lattice, Nature (London) **579**, 51 (2020).

[39] Y. Komijani, Isolating kondo anyons for topological quantum computation, Phys. Rev. B **101**, 235131 (2020).

[40] J. Wang and Y.-f. Yang, Nonlocal kondo effect and quantum critical phase in heavy-fermion metals, Phys. Rev. B **104**, 165120 (2021).

[41] R. Han, D. Hu, J. Wang, and Y.-f. Yang, Schwinger boson approach for the dynamical mean-field theory of the kondo lattice, Phys. Rev. B **104**, 245132 (2021).

[42] Y. Ge and Y. Komijani, Emergent Spinon Dispersion and Symmetry Breaking in Two-Channel Kondo Lattices, Phys. Rev. Lett. **129**, 077202 (2022).

[43] K. P. Stadler, Z. M. Yin, J. Von Delft, G. Kotliar, and A. Weichselbaum, Dynamical Mean-Field Theory Plus Numerical Renormalization-Group Study of Spin-Orbital Separation in a Three-Band Hund Metal, Phys. Rev. Lett. **115**, 136401 (2015).

[44] C. Varma, Z. Nussinov, and W. Van Saarloos, Singular or non-Fermi liquids, Phys. Rep. **361**, 267 (2002).

[45] P. Coleman and C. Pépin, Singular Fermi liquid behavior in the underscreened Kondo model, Phys. Rev. B **68**, 220405 (2003).
[46] P. Mehta, N. Andrei, P. Coleman, L. Borda, and G. Zarand, Regular and singular Fermi-liquid fixed points in quantum impurity models, Phys. Rev. B **72**, 014430 (2005).
[47] P. Coleman and I. Paul, Quantum replica approach to the underscreened kondo model, Phys. Rev. B **71**, 035111 (2005).
[48] P. Coleman, *Introduction to Many-Body Physics* (Cambridge University Press, Cambridge, England, 2015).
[49] P. Werner, E. Gull, and A. J. Millis, Metal-insulator phase diagram and orbital selectivity in three-orbital models with rotationally invariant Hund coupling, Phys. Rev. B **79**, 115119 (2009).
[50] N. Lanata, H. U. Strand, G. Giovannetti, B. Hellsing, L. De'Medici, and M. Capone, Orbital selectivity in Hund's metals: The iron chalcogenides, Phys. Rev. B **87**, 045122 (2013).
[51] F. B. Kugler, S.-S. B. Lee, A. Weichselbaum, G. Kotliar, and J. Von Delft, Orbital differentiation in Hund metals, Phys. Rev. B **100**, 115159 (2019).
[52] F. B. Kugler and G. Kotliar, Is the Orbital-Selective Mott Phase Stable Against Interorbital Hopping?, Phys. Rev. Lett. **129**, 096403 (2022).
[53] One could include realistic crystal field splitting effects in our model by breaking the degeneracy of the three orbitals. The isotropic holon energy term in Eq. (2) would become $\epsilon_f[X^{(1)}_{a,a} + X^{(1)}_{a,a}] + (\epsilon_f + \Delta_{cf})X^{(3)}_{a,a}$, which leads to an additional self-energy equation for the holons. We expect that a finite Δ_{cf} will lead to orbital differentiation, with different $T_{\rm orb}$ crossover temperatures for each orbital subset, but that the S.O.S. regime would remain. The detailed effects of such perturbations are beyond the scope of our work.
[54] P. Coleman, I. Paul, and J. Rech, Sum rules and Ward identities in the Kondo lattice, Phys. Rev. B **72**, 094430 (2005).
[55] E. Lebanon, J. Rech, P. Coleman, and O. Parcollet, Conserving many body approach to the infinite-U Anderson model, Phys. Rev. Lett. **97**, 106604 (2006).
[56] See Supplemental Material at http://link.aps.org/supplemental/10.1103/PhysRevResearch.4.L042011 for further information on the bare mixed valence problem, the derivation of spin and orbital susceptibilities, details on the single iteration approach, the scaling of the spin susceptibility and the quasi-power-law exponent.
[57] K. M. Stadler, A model study of strong correlations in Hund metals, Ph.D. thesis, lmu (2019).
[58] Another definition of $\hat{L}_\gamma = \sum L^{mm'}_\gamma X^m_{ab} X^{m'}_{ba}$ purely in terms of orbital charge can generically be written. For the antisymmetric L_γ matrices, this leads to an identically zerow operator.
[59] I. Affleck, A. W. W. Ludwig, H.-B. Pang, and D. L. Cox, Relevance of anisotropy in the multichannel Kondo effect: Comparison of conformal field theory and numerical renormalization-group results, Phys. Rev. B **45**, 7918 (1992).
[60] I. Affleck and A. W. W. Ludwig, Exact conformal-field-theory results on the multichannel Kondo effect: Single-fermion Green's function, self-energy, and resistivity, Phys. Rev. B **48**, 7297 (1993).
[61] P. Coleman, L. B. Ioffe, and A. M. Tsvelik, Simple formulation of the two-channel Kondo model, Phys. Rev. B **52**, 6611 (1995).
[62] A. Georges and A. M. Sengupta, Solution of the Two-Impurity, Two-Channel Kondo Model, Phys. Rev. Lett. **74**, 2808 (1995).
[63] O. Parcollet and A. Georges, Transition from Overscreening to Underscreening in the Multichannel Kondo Model: Exact Solution at Large N, Phys. Rev. Lett. **79**, 4665 (1997).
[64] O. Parcollet, A. Georges, G. Kotliar, and A. Sengupta, Overscreened multichannel SU (N) Kondo model: Large-N solution and conformal field theory, Phys. Rev. B **58**, 3794 (1998).
[65] W. Koller, A. C. Hewson, and D. Meyer, Singular dynamics of underscreened magnetic impurity models, Phys. Rev. B **72**, 045117 (2005).
[66] T.-H. Lee, A. Chubukov, H. Miao, and G. Kotliar, Pairing Mechanism in Hund's Metal Superconductors and the Universality of the Superconducting Gap to Critical Temperature Ratio, Phys. Rev. Lett. **121**, 187003 (2018).
[67] Y.-M. Wu, A. Abanov, and A. V. Chubukov, Pairing in quantum critical systems: Transition temperature, pairing gap, and their ratio, Phys. Rev. B **99**, 014502 (2019).
[68] In reality, G_χ has a frequency dependent behavior, as we saw in the rest of the paper, but it can be approximated as nearly instantaneous with respect to the other propagators.
[69] A. Migdal, Interaction between electrons and lattice vibrations in a normal metal, Sov. Phys. JETP **7**, 996 (1958).
[70] G. Eliashberg, Interactions between electrons and lattice vibrations in a superconductor, Sov. Phys. JETP **11**, 696 (1960).
[71] R. Combescot, Strong-coupling limit of eliashberg theory, Phys. Rev. B **51**, 11625 (1995).
[72] E.-G. Moon and A. Chubukov, Quantum-critical pairing with varying exponents, J. Low Temp. Phys. **161**, 263 (2010).
[73] Y. Wang, A. Abanov, B. L. Altshuler, E. A. Yuzbashyan, and A. V. Chubukov, Superconductivity near a Quantum-Critical Point: The Special Role of the First Matsubara Frequency, Phys. Rev. Lett. **117**, 157001 (2016).
[74] H. Miao, L.-M. Wang, P. Richard, S.-F. Wu, J. Ma, T. Qian, L.-Y. Xing, X.-C. Wang, C.-Q. Jin, C.-P. Chou, Z. Wang, W. Ku, H. Ding, Coexistence of orbital degeneracy lifting and superconductivity in iron-based superconductors, Phys. Rev. B **89**, 220503 (2014).